

Gravitational Radiation Capture between Unequal Mass Black Holes

Yeong-Bok Bae,^{1, 2, *} Hyung Mok Lee,^{1, 3, †} Gungwon Kang,^{4, ‡} and Jakob Hansen^{4, §}

¹*Astronomy Program Department of Physics and Astronomy,*

Seoul National University, 1 Gwanak-ro, Gwanak-gu, Seoul 08826, Korea

²*Korea Astronomy and Space Science Institute, 776 Daedeokdae-ro, Yuseong-gu, Daejeon 34055, Korea*

³*Center for Theoretical Physics, Seoul National University, 1 Gwanak-ro, Gwanak-gu, Seoul 08826, Korea*

⁴*Supercomputing Center at KISTI, 245 Daehak-ro, Yuseong-gu, Daejeon 34141, Korea*

(Dated: December 3, 2024)

The gravitational radiation capture between unequal mass black holes without spins has been investigated with numerical relativistic simulations, and the results are compared with the Post-Newtonian (PN) approximations. We adopt the parabolic approximation which assumes that the gravitational wave radiation from a weakly hyperbolic orbit is the same as that from the parabolic orbit having the same pericenter distance. Using the radiated energies from the parabolic orbit simulations, we have obtained the impact parameters (b) of the gravitational radiation captures for weakly hyperbolic orbits as a function of initial energy. The most energetic encounters occur around the boundary between the direct merging and the fly-by orbits, and could emit several percent of the total ADM initial energy even from such fly-by orbits. Energy and angular momentum radiated in the case of unequal mass black holes are smaller than those of equal mass black holes at the same initial orbital angular momentum provided that their total masses are the same. We show that the agreement for impact parameters between the PN approximation and the numerical relativity begins to break down as encounter becomes very close (e.g., $b \lesssim 100$ M), and that disagreement becomes more conspicuous at higher mass ratios. For instance, the impact parameters could differ over 50% from those in the PN approximation if the impact parameter is $b \lesssim 30$ M for the mass ratio of $m_1/m_2 = 16$.

I. INTRODUCTION

Black hole (BH) binary merger has been regarded as one of the most promising sources of gravitational waves (GWs), and recently two such events were eventually observed by the advanced LIGO [1, 2]. One of the formation processes of the compact BH binary is a gravitational radiation capture (GR capture, hereafter) which occurs from close encounters between two BHs in very dense stellar systems such as globular clusters and galactic nuclei [3, 4]. Capture takes place when the amount of energy radiated by gravitational waves during the encounter becomes larger than the initial orbital energy.

Most studies on GR capture are based on Post-Newtonian (PN) order of 2.5 (2.5 PN) by Peters [5] and Hansen [6]. Peters [5] calculated the amount of gravitational radiation from two point masses assuming bound Keplerian orbits, and Hansen [6] extended this work to hyperbolic Keplerian orbits. Quinlan and Shapiro [7, 8] have obtained the cross section of GR capture based on Peters [5]’s results.

PN calculations of GR capture can be applied for the most cases of BH encounters whose orbital energy is much smaller than the rest-mass energy, i.e., non-relativistic cases. However, if the pericenter distance is extremely small, the full relativistic treatments are required because the PN approximation would lead to large errors.

Since the amount of energy that has to be dissipated for capture is approximately $3/2\mu\sigma^2$, where μ is the reduced mass and σ is the one-dimensional velocity dispersion of the cluster, the deviation from PN is expected for systems with very large σ . The velocity dispersion for typical star clusters such as globular clusters and open clusters is less than a few tens of km s^{-1} and a few hundred km s^{-1} for the central parts of the galaxies. Therefore PN approximation is generally sufficient for GR captures in those clusters. However, most of the galaxies are known to harbor supermassive BHs whose masses are proportional to the masses of host galaxies (e.g., [9–12]). Stars around the BH up to the radius of influence follow cuspy density distribution of $r^{-7/4}$ for the case of single mass [13]. The velocity dispersion also follows a power-law of $r^{-1/2}$, implying the possibility of very large value at very small distances from the central BH. If there exists a mass function, the density profile of more massive components is expected to be steeper than the case of single mass case (e.g., [14]). Therefore, the encounters between stellar mass BHs in the galactic nuclei may be with very large relative velocity.

One of the interesting consequences of BH captures by GR is the possibility of forming very eccentric binaries. Note that most BH binaries are expected to be circularized before the merging [5, 15] due to the loss of the orbital energies during the inspiral phase, thus the analyses of GW data and the parameter estimations of GW sources have focused on the circular orbit without the eccentricity. However, the typical deviation of eccentricity from 1 of the captured binaries can be of order of $1 - e \approx 6.5 \times 10^{-3} \eta^{2/7} (\sigma/1000 \text{ km s}^{-1})^{10/7}$ where

* baeyb@astro.snu.ac.kr

† hmlee@snu.ac.kr

‡ gwkang@kisti.re.kr

§ jakob@jakobonline.dk

$\eta \equiv m_1 m_2 / (m_1 + m_2)^2$ is the symmetric mass ratio [4]. On the other hand, typical pericenter of the captured binaries is $r_p \approx 5.7 \times 10^2 (\sigma/1000 \text{ km s}^{-1})^{-4/7} \text{ km}$ for the $10 M_\odot$ BH pairs [4]. Thus, if the velocity dispersion reaches to $\sigma = 1000 \text{ km s}^{-1}$, the corresponding pericenter is just about 20 Schwarzschild radii. Consequently the captured binaries in dense stellar systems with high velocity dispersion can merge and radiate gravitational waves while possessing significant eccentricity. The formation process of such extreme binaries may require full general relativistic numerical simulations.

The purpose of the present study is to extend the numerical simulations of close encounters between two BHs to the case of unequal masses. The previous study by Hansen *et al.* [16] made very detailed numerical simulations of GR capture of equal mass BH encounters. However, stellar mass BHs are known to have wide mass spectrum ranging from a few to several tens of solar masses, as evident from the X-ray binaries and GW150914. Encounters between unequal mass BHs would be more common than equal mass cases.

The outline of this paper is as follows. In section II, the details of our relativistic simulations—the assumptions, the software we have adopted and the configurations of initial conditions etc.—are described. In section III, the convergences of our simulations are tested, and in section IV, the main results of our simulations about GR capture with unequal mass BHs are presented. The cross sections of GR capture are also calculated. In section V, the validity of parabolic approximation we employ is verified, and in section VI the application of relativistic GR capture is discussed.

II. NUMERICAL SETUP

In order to simulate the GR capture process, we need to follow hyperbolic orbits with positive initial energy. There exist two conservative quantities for hyperbolic orbits in non-relativistic limit: orbital energy and angular momentum. Since we do not know these quantities for orbits that lead to the capture, large number of full simulations are required just to determine the initial orbit. However, it would be difficult to do so with limited computational resources.

Therefore, we adopt the parabolic approximation. It assumes that the weakly hyperbolic orbit emits the same amount of energy with the parabolic orbit of the same pericenter distance, because both orbits have almost same paths around the pericenter where most GWs are radiated. If we know the radiated energy from the parabolic orbit, we can consider that the hyperbolic orbit with the orbital energy less than that can be captured by GW radiation because it would emit the same amount of energy with the parabolic orbit. Thus the radiated energy from the parabolic orbit can be regarded as the upper limit of the orbital energy of the hyperbolic orbit leading to the capture. Under the parabolic approxima-

tion, we can compute the radiated energy as a function of initial angular momentum (or pericenter distance) from the parabolic orbit, and obtain the critical impact parameter for capture for a given initial velocity at infinity in the hyperbolic orbit. Quinlan and Shapiro [7, 8] also calculated the cross section of GR capture based on the parabolic approximation by pushing the limit of GW radiation of elliptical orbit in PN [5] to the parabolic orbit.

Here the initial parabolic orbit can be found by the constraining ADM mass [17]. The ADM mass is defined in the asymptotically flat space-time as the total mass-energy measured within a spatial infinite surface at any instant of time, and in Newtonian limit the ADM mass can be expressed as the summation of the rest mass and the orbital energy. The orbital energy of the parabolic orbit is zero in Newtonian limit, thus the initial parabolic orbit can be obtained by setting the ADM mass to be unity in the relativistic simulation.

In this study, the geometrized unit system is adopted to express the physical quantities. The speed of light in vacuum c and the gravitational constant G are set to be unity in the geometrized system, and the length, time, mass and energy are expressed with the units of mass M .

We use Einstein Toolkit[18] which is open to the public for fully general relativistic simulations and adopt the standard thorns and settings (1+log lapse, Gamma-driver shift etc.). The initial data are constructed using TwoPuncture thorn[19] similar to the previous study of equal mass encounters [16]. Initially two BHs are located on the x-axis with their center of mass at the origin. Then for the fixed initial angular momentum (i.e., for the fixed y-direction linear momentum), the linear momentum of x-direction and the puncture mass are determined with the total ADM [17] mass of unity. The initial distance between two BHs has to be sufficiently large to reduce the junk radiation and separate that from the true GW signals. In our simulations, the initial separation of two BHs is set to be 60 M in the geometrized unit.

Ideally the GWs should be extracted at infinity but that is not possible in numerical simulations. Thus, we have to extract them at finite but sufficiently large distances where the BH system can be recognized as a point mass to get sufficiently accurate GWs. For the parabolic orbit with larger pericenter distance, the extraction radii have to be correspondingly larger because the effective size of the BH system is larger. Additionally, the unequal mass system does not have rotational symmetry contrary to the equal mass system. This means that the simulation domain has to be twice of the equal mass system. Spatial resolution requirement also becomes more stringent for unequal mass case than equal mass case since the minimum spatial grid has to be determined by the lower mass BH. Consequently, much more computer resources are required for the simulations of the unequal mass BHs than those of the equal mass BHs.

In order to overcome this resource problem, we adopt the multiblock infrastructure, Llama code[20]. In a Cartesian coordinate, we can use a mesh refinement

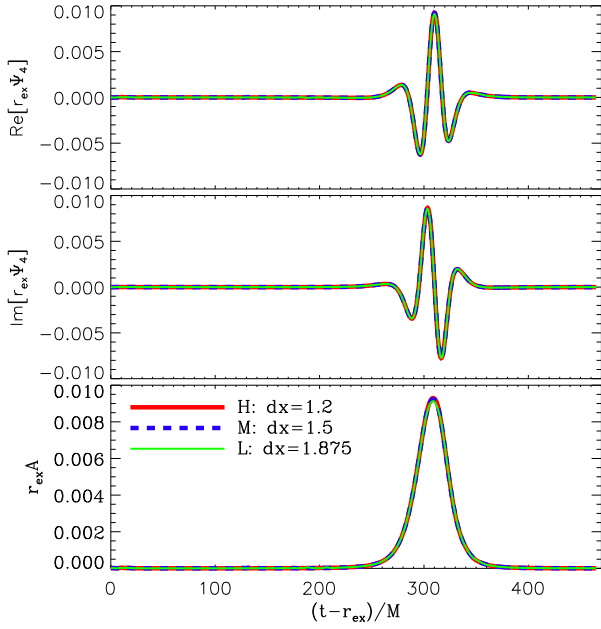


FIG. 1. Comparison of Ψ_4 and amplitudes for three different resolutions. The mass ratio is $m_1/m_2 = 4$ and the initial angular momentum is $L_{\text{init}} = 0.64$.

based on ‘Carpet’ in Cactus. But the expansion of the simulation domain is very expensive because the number of grid points is proportional to the cube of the length scale. If we want to expand the simulation domain twice, the required number of grid points increases about 8 times. However, if we can use the spherical-like coordinate, the required number of grid points is just proportional to the length scale, provided that the number of angular grid points is fixed. The Llama code [20] enables us to use both coordinates in the simulation domain. The Cartesian coordinate is adopted for the central region where the mesh refinement is required around the BHs, while the spherical-like coordinate is used for the outer region where the GWs are extracted. Information on different patches are shared by the interpolation in the overlapped grids. Consequently, we can expand the simulation domain much farther with less computational resources.

In this study, we adopt 7 patches system which is composed of central Cartesian coordinate and 6 spherical-like patches attached on each face of the Cartesian cube. Unlike the quasi-circular merging simulations, two BHs can reach far region after the encounter, thus the central patch where we can use the mesh refinement around the BHs has to be large enough to encompass two BHs. Inner radii of spherical-like coordinates are set to be 80 M–120 M depending on the cases. Outer boundaries of spherical-like coordinates are set to be larger than 1200 M to avoid the errors caused by the wave reflection from the outer boundary.

In the previous study of equal-mass BHs [16], the finest

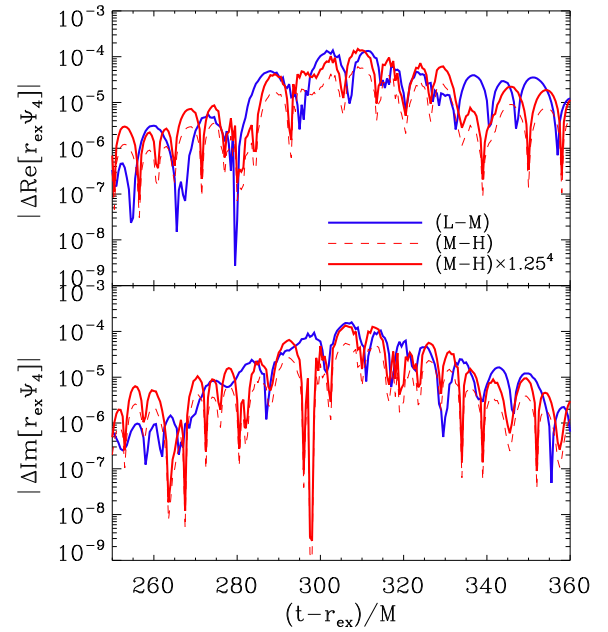


FIG. 2. The absolute values of the differences of $\Psi_4(l = 2, m = 2)$ between the different resolutions. Here, we have selected the time range around the peak point in the amplitudes (Fig. 1). The differences (L-M) is nearly overlapped with (M-H) if (M-H) is multiplied by 1.25^4 .

grid size was $1.1/64$ M. However, higher resolutions are required for the low mass BH in the unequal mass BH simulations. In this study, the finest grid sizes have been determined by considering the puncture mass and the apparent horizon size in an inversely proportional manner, and have been set to be $1.25/128$ M, $1.5/256$ M, $1.8/512$ M and $1.0/512$ M for the mass ratios of 2, 4, 8 and 16 respectively.

Weyl scalar Ψ_4 which is equal to the second time derivatives of two polarizations of the GWs in Newman-Penrose formalism is extracted using WeylScal4 and decomposed into the spin-weighted spherical harmonics with Multipole thorns [21] that are included in Einstein Toolkit. We set the various extraction radii in the range of 120 M–500 M depending on the pericenter distances. Farther extraction radii are used for the large initial angular momentum cases because they have distant pericenter. The radiated energy and angular momentum are calculated by extrapolating the integration of GWs at each extraction radius.

III. CONVERGENCE TEST

In order to check that we are using the appropriate resolutions, the convergence should be tested with the different grid sizes. Since we have several models with different mass ratios and initial angular momenta, it is not possible to check the convergences for all the mod-

els. We have selected the representative case of close fly-by orbit ($L_{\text{init}} = 0.64$) with the intermediate mass ratio $m_1/m_2 = 4$.

Three different resolutions $dx = 1.875/256 \text{ M}, 1.5/256 \text{ M}$ and $1.2/256 \text{ M}$ are adopted where ‘ dx ’ is the finest grid size. Hereafter, the letters ‘L’, ‘M’ and ‘H’ represent the low ($dx = 1.875/256 \text{ M}$), medium ($dx = 1.5/256 \text{ M}$) and high ($dx = 1.2/256 \text{ M}$) resolutions. The ratio of grid size between ‘L’ and ‘M’, and ‘M’ and ‘H’ is 1.25, and the box sizes of the mesh refinement levels are set identically.

Figure 1 shows the real and imaginary parts of the Weyl scalar Ψ_4 in $(l, m) = (2, 2)$ mode, and the amplitudes of them. For the comparison, the Ψ_4 and amplitudes are multiplied by the extraction radius r_{ex} , and measured at the retarded time. Since they show almost the same behaviours, we have subtracted one from the other to see the differences in detail. Figure 2 shows the absolute values of the differences of Ψ_4 between ‘L’ and ‘M’ (L-M), and ‘M’ and ‘H’ (M-H) around the peak point of the amplitudes. We can see that the difference (M-H) is smaller than (L-M). We also compared (L-M) with (M-H) multiplied by 1.25⁴ and found that they agree well. This result confirms the fourth order convergence in grid.

The medium resolution ($dx = 1.5/256 \text{ M}$) is adopted in the following simulations for the mass ratio $m_1/m_2 = 4$, because it is considered to be sufficient for this study. The difference of the radiated energies between the medium and high resolutions is only 0.1%.

Note that the convergence test is just for the representative model, the mass ratio $m_1/m_2 = 4$. However, the resolutions for the other models are also adjusted in similar manner based on the puncture mass and the size of the apparent horizon. Therefore, the resolutions for the other models are also considered to be within the convergent ranges.

IV. RESULTS

We have performed the parabolic orbit simulations for the different mass ratios up to $m_1/m_2 = 16$. Since the ADM mass of the parabolic orbit is fixed, we only need to specify the initial angular momentum (L_{init}) to describe the orbit for a given mass ratio. Here, the initial angular momentum is calculated by $L_{\text{init}} = x_1 p_{y,1} + x_2 p_{y,2}$ where x_1, x_2 are the positions of two BHs on the x-axis and $p_{y,1}, p_{y,2}$ are the linear momenta in y-directions.

Several simulations are shown in Fig. 3 with the mass ratio of $m_1/m_2 = 4$. Upper panel shows the orbits of heavier BHs. They are drawn from their separations of 35 M and aligned to start from the same point for easier comparison. The orbits of lower mass BHs, in the opposite side with four times farther distances, are omitted for convenience. Lower panel shows the GWs from those orbits.

At large L_{init} , two BHs show fly-by orbit without merging. They are in bound state, but their apocenter is too far to be simulated. As the L_{init} decreases, BHs end up

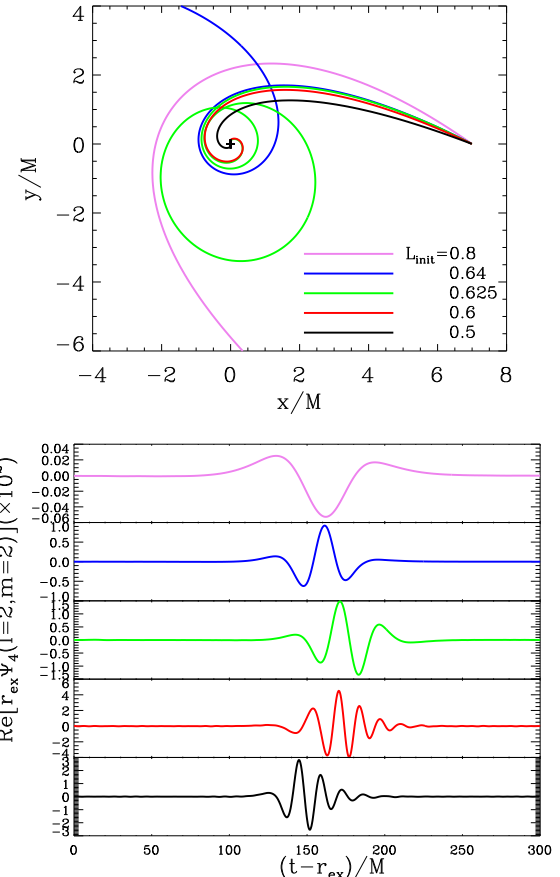


FIG. 3. Upper panel shows the orbit of heavier BHs with different initial angular momenta when the mass ratio $m_1/m_2 = 4$. Lower panel is the real part of Ψ_4 multiplied by the extraction radii (r_{ex}). Same color represents the same L_{init} .

with more tightly bound orbit (e.g., $L_{\text{init}} = 0.625$). BHs merge nearly directly for two other cases of smaller L_{init} (0.6 and 0.5). Note that the scales of the vertical axes in the lower panel are different from each other. As the L_{init} decreases, the amplitude of Ψ_4 becomes larger, and it has the largest value on the boundary between the fly-by and direct merging orbits. If we reduce L_{init} further, the amplitude becomes smaller again.

In this study, we want to obtain the marginal energy of the GR capture through the parabolic simulations. The information we need is the radiated energy from just one-passage in the parabolic orbit. Therefore, the direct merging orbit cannot be used for calculating the marginal energy of GR capture process.

A. Radiated Energy & Angular Momentum

We have measured the radiated energies (E_{rad}) and angular momenta (L_{rad}) of encounters on parabolic orbits with different mass ratios. We have integrated Ψ_4 up to

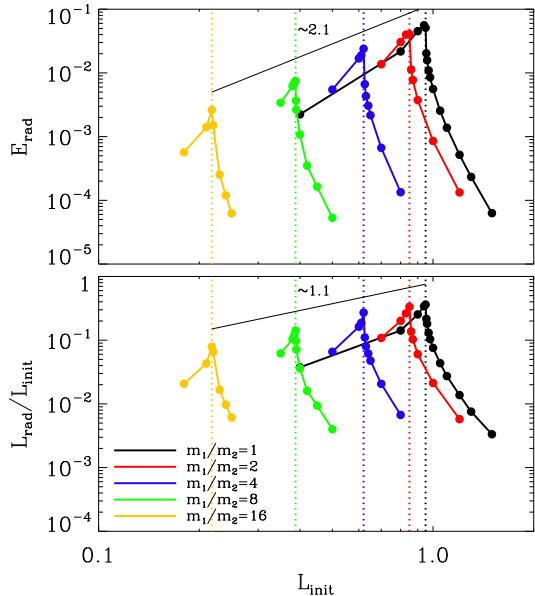


FIG. 4. The radiated energy E_{rad} and angular momentum L_{rad} with different mass ratios. L_{rad} is divided by the initial angular momentum L_{init} to represent the radiation fraction. E_{rad} is the radiation fraction itself, because the initial ADM energy is 1. The dotted lines are the boundaries between the direct merging and the fly-by orbit. Thin black solid lines represent the linear fitting of the peak points with their slopes in logarithmic scale.

$l = 12$ modes in multipole expansions to calculate E_{rad} and L_{rad} .

Figure 4 shows the E_{rad} and L_{rad} as a function of the initial angular momentum (L_{init}) for five different mass ratios. There are peak points both in E_{rad} and L_{rad} for each mass ratio. In the left hand side of the peak, including the peak point itself, two BHs merge directly. The E_{rad} and L_{rad} in this part are integrated results up to the merger. On the other hand, the right hand side of the peak is from the fly-by orbits, where we calculate E_{rad} and L_{rad} for one-passage. Regardless of the mass ratio, the orbit on the boundary between the direct merging and the fly-by gives the largest amount of GW radiations. As the initial angular momentum deviates further from this boundary, the GW radiation drops quickly, especially for the fly-by orbits.

As the mass ratio becomes large, the boundary between the direct merging and the fly-by orbit shifts to the lower initial angular momenta (Fig. 4). These L_{init} at the peak are roughly proportional to the reduced mass $\mu = m_1 m_2 / (m_1 + m_2)$, which means the specific initial angular momenta at the peak are almost the same. In addition, the radiated energies and angular momenta at the peak follow the power law with E_{rad} , $L_{\text{rad}} \propto L_{\text{init}}^{2.1}$. However, we should be careful to extrapolate these results to the higher mass ratio, because the peak points cannot be defined precisely. Near the boundaries, BHs can have whirling orbits around each other, and for these

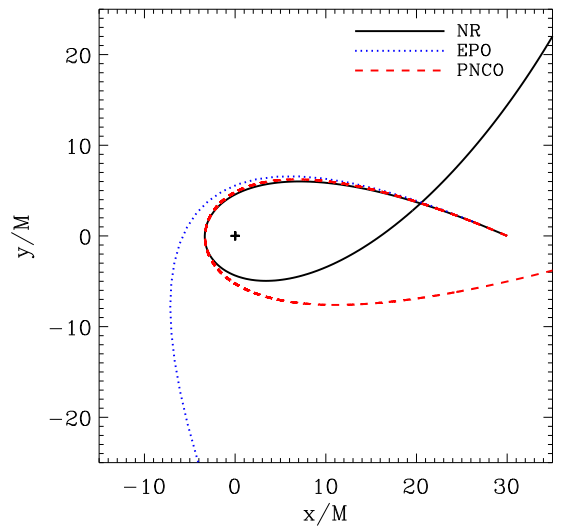


FIG. 5. The comparison of the exact parabolic orbit (EPO), PN corrected orbit (PNCO) and the orbit from numerical relativity (NR). The mass ratio is 1 and the initial angular momentum is $L_{\text{init}} = 1.1$. Here, we present the orbit of one BH. The other is opposite side of the origin.

cases it is difficult to discriminate one-passage from the orbit.

The results from the numerical simulations are compared with those of the PN. According to the parabolic approximation, the radiated energy from the parabolic orbit is given by [7, 8]

$$\Delta E = \frac{85\pi}{12\sqrt{2}} \frac{G^{7/2}}{c^5} \frac{m_1^2 m_2^2 (m_1 + m_2)^{1/2}}{r_p^{7/2}}, \quad (1)$$

where G and c are gravitational constant and speed of light, respectively, and r_p represents a pericenter distance of the parabolic orbit. The GR capture will occur if the orbital energy is less than ΔE . If we use the relation between r_p and angular momentum L as $r_p = (m_1 + m_2)L^2/2Gm_1^2m_2^2$, the Eq. (1) can be rewritten as

$$\Delta E = \frac{170\pi}{3} \frac{G^7}{c^5} \frac{m_1^9 m_2^9}{(m_1 + m_2)^3} \frac{1}{L^7}. \quad (2)$$

In a similar way, the radiated angular momentum ΔL can be expressed with the orbital angular momentum L ,

$$\Delta L = 24\pi \frac{G^5}{c^5} \frac{m_1^6 m_2^6}{(m_1 + m_2)^2} \frac{1}{L^4}. \quad (3)$$

Now we have obtained the expression of radiated energy and angular momentum with respect to the initial angular momentum ($L = L_{\text{init}}$), thus we can compare these results directly with those from the numerical relativity (NR).

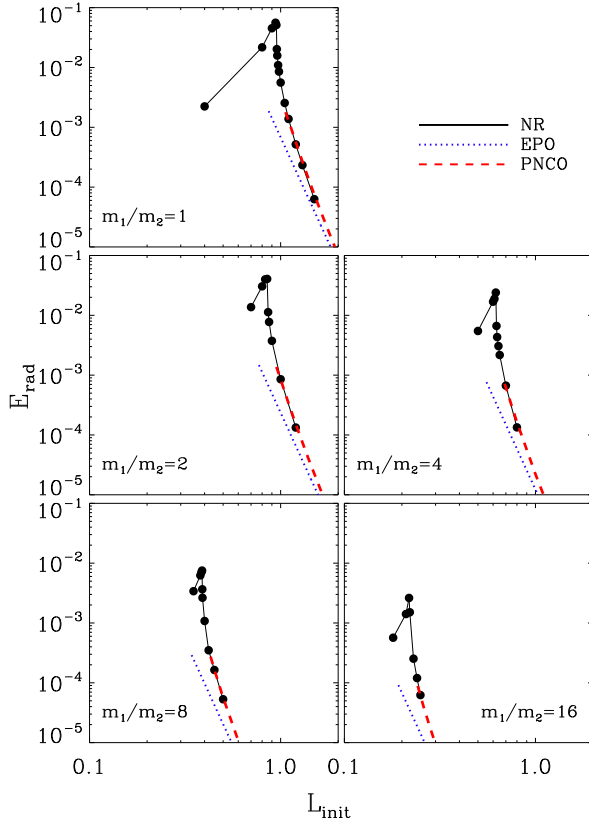


FIG. 6. The comparison of the radiated energy from the relativistic simulations (solid lines) with PNs. Dotted lines are from the exact parabolic orbits (EPOs, Eq. 2) and the dashed lines are from the PN corrected orbits (PNCOs).

In computing the above formula, the orbit is assumed to remain parabolic from the initial to the final stages. However, the exact parabolic orbit (EPO) is not possible in practice. During the encounter, the orbit changes gradually due to the gravitational radiation. In order to compare our numerical results with the PN approximation in a more consistent manner, we should take into account the corresponding changes of the orbit.

We have used a code [22] for two body motions written by S. J. Aarseth and we have added the PN correction terms up to 3.5 PN order for non-spinning case [23]. The time derivatives of the acceleration terms should also be added because it adopts the Hermite integration schemes. Along the orbit, we have calculated the radiated energy and angular momentum by using the mass quadrupole formula. The initial separation of two BHs is 10^4 M on parabolic orbit.

Figure 5 shows the exact parabolic orbit (EPO), PN corrected orbit (PNCO) and NR orbit. Compared to the EPO, the PNCO and the NR orbits are more tightly wound. Particularly near the pericenter where most GWs are generated, PNCO and NR orbits have almost same paths. Therefore, we can expect that the PNCO will pro-

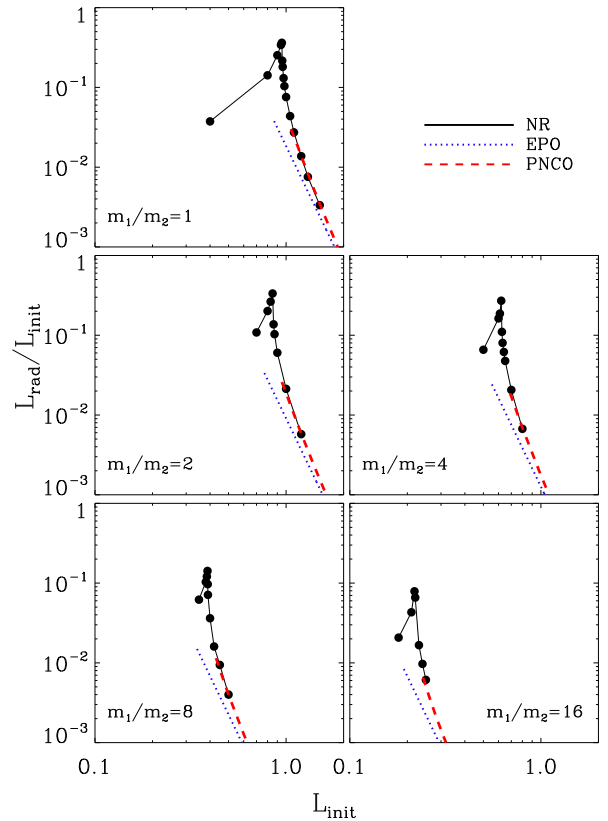


FIG. 7. The comparison of the radiated angular momentum from the relativistic simulations (solid lines) with PNs. Dotted lines are from EPOs (Eq. 3) and the dashed lines are from PNCOs.

vide more accurate quantities about the GW radiations than the EPO.

Figures 6 and 7 show the comparisons of the radiated energies and angular momenta between the NR and the PN. Dotted lines are the GW radiation from the EPOs in Eq. (2) and (3), and dashed lines represent the GW radiations from the PNCOs. The radiated energy and angular momentum of EPO and PNCO are calculated up to those with pericenter distance of 6 M.

Around the initial angular momentum of peak points, NR gives much larger radiated energy and angular momentum by an order of magnitude than EPO (dotted lines). On the other hand, the PNCOs (dashed lines) provide much more consistent results as expected from Fig. 5 at least for the orbits with $r_p \gtrsim 6$ M.

B. Critical Impact Parameters for Capture

In the Newtonian limit, the angular momentum L and the energy E of the hyperbolic orbit are given as follows,

$$L = b \mu v_\infty, \quad (4)$$

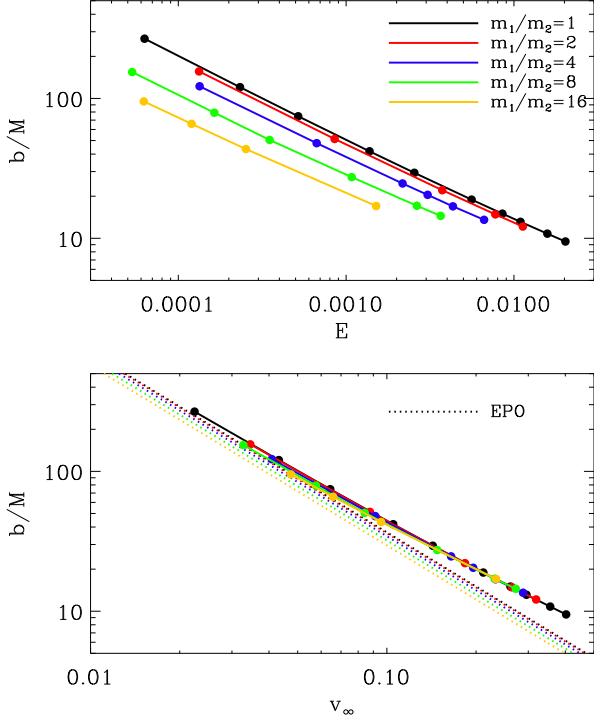


FIG. 8. The impact parameters from NR simulations as a function of the energy (upper) and the relative velocity at infinity (lower). NR results deviate from the EPO's in high velocity region.

$$E = \frac{1}{2} \mu v_\infty^2, \quad (5)$$

where b is impact parameter, μ is reduced mass and v_∞ is relative velocity between two BHs at infinity. From these equations, the impact parameter can be expressed with the energy and angular momentum of the hyperbolic orbit as follows,

$$b = \frac{L}{\mu v_\infty} = \frac{L}{\sqrt{2\mu E}}. \quad (6)$$

The parabolic approximation uses the physical quantities of the parabolic orbit instead of those of the hyperbolic orbit. The hyperbolic orbit whose orbital energy is less than the radiated energy gives GR capture. Therefore, the impact parameter of the marginally capturing orbit can be obtained if we substitute the radiated energy E_{rad} and initial angular momentum L_{init} in the parabolic orbit simulations for E and L in Eq. (6).

The upper panel of Fig. 8 shows the comparison of the impact parameters from NR simulations of different mass ratios as a function of E . Since it is more difficult to capture the BHs with high energy, their impact parameters are smaller. As the mass ratio increases, the impact parameter decreases for a given energy.

It is more intuitive to express the impact parameter in terms of v_∞ . For EPO, we get b as a function of v_∞

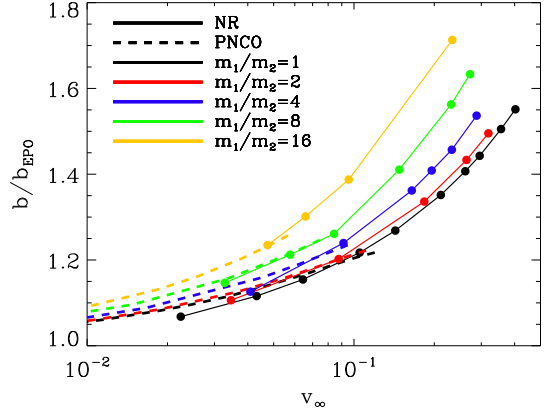


FIG. 9. The comparison of the impact parameters from different methods. The impact parameters are divided by those of the EPO.

using Eq. (2), (4), and (5),

$$b = \left(\frac{340\pi}{3} \frac{m_1 m_2 (m_1 + m_2)^5}{v_\infty^9} \right)^{1/7}. \quad (7)$$

According to this equation, the impact parameter has very weak dependence on the masses. It is proportional to $(m_1 m_2)^{1/7}$ if the total mass is fixed. NR results show even weaker dependence than this, i.e., nearly independent of the mass ratio (lower panel of Fig. 8). However, their slopes are less steep compared to the EPO's ($b \propto v^{-9/7}$). NR always gives larger impact parameters than EPO's especially in the high velocity region.

Figure 9 shows the critical impact parameters from PNCO and NR normalized by that of EPO. The EPO approximation which uses the results of Peters [5] gives consistent impact parameters with NR and PNCO up to $v_\infty \sim 0.01$ within about 10%. Therefore, it is suitable for the GR captures in globular clusters or nuclear star clusters [3, 4, 8] where the velocity dispersions are generally smaller than 0.01.

As the velocity becomes larger, the deviations from the EPO's also become larger for both PNCO and NR. However, the PNCO shows similar impact parameters with NR up to $v_\infty \sim 0.1$. In the higher velocity region, the NR gives larger impact parameter—over 50%—than EPO's. The GR capture process in higher energy region requires more exact treatments for the relativistic effects. Their orbits deviate from EPO significantly, and the relativistic effects become important. The BH cannot be treated as a point mass either. The deviation is more conspicuous for the high mass ratio system. Therefore, the orbital changes due to the general relativistic effects should be considered more seriously, especially for the high mass ratio systems.

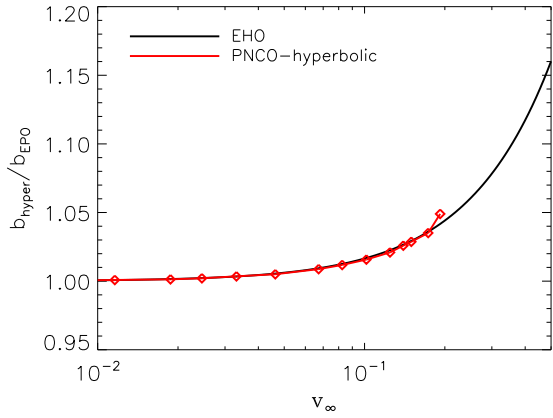


FIG. 10. The impact parameters from the exact hyperbolic orbit (EHO) and PN corrected hyperbolic orbit (PNCO-hyperbolic) with respect to the exact parabolic orbit (EPO). These are equal mass and non-spinning cases.

V. VALIDITY OF PARABOLIC APPROXIMATION

In this study, we have adopted the parabolic approximation which uses the parabolic orbit instead of the hyperbolic orbit for the simulations of GR capture. But obviously, the parabolic approximation implicitly assumes that the orbits are only weakly hyperbolic, i.e., orbital energy is much smaller than rest-mass energy. Therefore, it is important to check the validity of the parabolic approximation for the high velocity encounters. As mentioned in section II, to find the hyperbolic orbit that gives marginal capture is very time consuming in NR because of the additional parameter (i.e., energy) to specify the orbits. Therefore, we will use the PN approaches which do not require heavy calculations for that.

For the exact hyperbolic orbit (EHO), similarly with the exact parabolic orbit (EPO), we can obtain the impact parameter of GR capture directly by using Hansen [6]'s results by equating the initial orbital energy with the radiated energy (Eq. (13)–(17) in Hansen [6]).

The PN corrected hyperbolic orbit can be calculated in the same way with the parabolic orbit by using the PN equation of motion. We have repeated the PNCO calculations until the difference between the initial orbital energy and the radiated energy becomes less than 0.01% of the initial orbital energy.

Figure 10 shows the impact parameters from the exact hyperbolic orbit (EHO) and PN corrected hyperbolic orbit (PNCO-hyperbolic) normalized by that of exact parabolic orbit (EPO). We found that $b_{\text{hyper}}/b_{\text{EPO}}$ remains below 1.05 for both EHO and PNCO-hyperbolic cases up to $v_{\infty} \sim 0.2$. This means the parabolic approximation is valid within 5% for that v_{∞} range. For the encounters with even higher velocity, the hyperbolic orbit gives larger deviations from the parabolic orbit, which

implies that true impact parameters of hyperbolic orbit can be at least 5% larger than that based on the parabolic approximations at $v_{\infty} \gtrsim 0.2$. NR would give qualitatively similar results.

VI. DISCUSSIONS

We have carried out detailed studies of GR capture between two BHs using NR. We have employed parabolic approximation for the initial orbits and found that such an approximation is applicable for the encounters with relative velocity up to $10 \sim 20$ % of the speed of light.

As mentioned in section I, the velocity dispersion could become very large in the vicinity of the supermassive BHs. O'Leary *et al.* [3] argued that the encounters between relatively massive stellar mass BHs near the supermassive BH of the galactic nuclei could be quite frequent. Some of them would occur with very large relative velocity, although majority are still expected at lower velocities. Therefore, the galactic center near the supermassive BH is the most probable place of the relativistic encounters.

However, we should note that v_{∞} we obtained is the 'maximum' relative velocity at infinity to be captured by GW radiation at a fixed impact parameter. If v_{∞} of the hyperbolic orbit is less than that, the pericenter distance will be smaller or two BHs will merge directly, which means that the encounter becomes more relativistic. Therefore, v_{∞} is not the only factor for the relativistic encounter. The initial angular momentum L_{init} which is the multiplication of v_{∞} and b (Eq. 4) determines whether the encounter is relativistic (Fig. 4).

The signature of the strong relativistic encounters would be the GWs coming from very eccentric mergers. Such events would be rare but even a few events will tell us about the physical conditions where they were born.

The GR capture with very high mass ratio such as the supermassive BH and the stellar mass BH also requires more exact relativistic treatments. The impact parameter between them can be much larger than what we expect in EPO. The mass ratios in this study are limited to 16, but we have seen that the deviation of impact parameter of high mass ratio from EPO begins at lower relative velocity and is getting larger than that of low mass ratio. Therefore, the EPO should be used very carefully for those cases even though their relative velocity is not larger than 0.01.

In the present study we have not considered spin of the BHs. In very close encounters between BHs spin is expected to play important roles. We will return this subject in the forthcoming paper.

VII. ACKNOWLEDGEMENTS

YB and HML were supported by NRF grant number NRF-2006-0093852 funded by the Korean government

and partially by the KISTI-GSDC's cooperative Program (K-16-L01-C06-S01). GK was supported in part by the R&D Program of KISTI (K-16-L05-C01-S01) and the Academic Program of APCTP. The computation was

carried out with the supercomputer and technical supports in KISTI through the HPC application program (KSC-2014-C3-017, KSC-2014-C3-065).

[1] B. P. Abbott, R. Abbott, T. D. Abbott, M. R. Abernathy, F. Acernese, K. Ackley, C. Adams, T. Adams, P. Addesso, R. X. Adhikari, and et al., *Physical Review Letters* **116**, 061102 (2016), arXiv:1602.03837 [gr-qc].

[2] B. P. Abbott, R. Abbott, T. D. Abbott, M. R. Abernathy, F. Acernese, K. Ackley, C. Adams, T. Adams, P. Addesso, R. X. Adhikari, and et al., *Physical Review Letters* **116**, 241103 (2016), arXiv:1606.04855 [gr-qc].

[3] R. M. O'Leary, B. Kocsis, and A. Loeb, *Mon. Not. R. Astron. Soc.* **395**, 2127 (2009), arXiv:0807.2638.

[4] J. Hong and H. M. Lee, *Mon. Not. R. Astron. Soc.* **448**, 754 (2015), arXiv:1501.02717.

[5] P. C. Peters, *Physical Review* **136**, 1224 (1964).

[6] R. O. Hansen, *Phys. Rev. D* **5**, 1021 (1972).

[7] G. D. Quinlan and S. L. Shapiro, *Astrophys. J.* **321**, 199 (1987).

[8] G. D. Quinlan and S. L. Shapiro, *Astrophys. J.* **343**, 725 (1989).

[9] L. Ferrarese and D. Merritt, *Astrophysical Journal Letters* **539**, L9 (2000), astro-ph/0006053.

[10] S. Gillessen, F. Eisenhauer, S. Trippe, T. Alexander, R. Genzel, F. Martins, and T. Ott, *Astrophys. J.* **692**, 1075 (2009), arXiv:0810.4674.

[11] R. Genzel, F. Eisenhauer, and S. Gillessen, *Reviews of Modern Physics* **82**, 3121 (2010), arXiv:1006.0064.

[12] J. Kormendy and L. C. Ho, *Annual Review of Astronomy and Astrophysics* **51**, 511 (2013), arXiv:1304.7762.

[13] J. N. Bahcall and R. A. Wolf, *Astrophys. J.* **209**, 214 (1976).

[14] T. Alexander and C. Hopman, *Astrophys. J.* **697**, 1861 (2009), arXiv:0808.3150.

[15] R. M. O'Leary, F. A. Rasio, J. M. Fregeau, N. Ivanova, and R. O'Shaughnessy, *Astrophys. J.* **637**, 937 (2006), astro-ph/0508224.

[16] J. Hansen, G. Kang, H. Kim, P. Diener, and F. Löffler, “Gravitational Radiation Captures of Black Holes in Weakly Hyperbolic Orbits,” to be submitted.

[17] R. L. Arnowitt, S. Deser, and C. W. Misner, “Canonical analysis of general relativity,” in *Recent Developments in General Relativity* (1962) p. 127.

[18] “Einstein toolkit - <http://einstein toolkit.org/>” .

[19] M. Ansorg, B. Brügmann, and W. Tichy, *Phys. Rev. D* **70**, 064011 (2004), gr-qc/0404056.

[20] D. Pollney, C. Reisswig, E. Schnetter, N. Dorband, and P. Diener, *Phys. Rev. D* **83**, 044045 (2011), arXiv:0910.3803 [gr-qc].

[21] J. Baker, M. Campanelli, and C. O. Lousto, *Phys. Rev. D* **65**, 044001 (2002), gr-qc/0104063.

[22] “<http://www.ast.cam.ac.uk/sverre/web/pages/nbody.htm>,” .

[23] L. Blanchet, *Living Reviews in Relativity* **17** (2014), 10.12942/lrr-2014-1, arXiv:1310.1528 [gr-qc].